ԳԻՏՈՒԹՅՈՒՆ

Հեռ.՝ + 374 (55) 78 47 87
+ 374 (95) 53 96 47
E-mail:lusabatsgm@gmail.com

ՀՀ ԳԱԱ Ա.Բ. ՆԱԼԲԱՆԴՅԱՆԻ ԱՆՎԱՆ ՔԻՄԻԱԿԱՆ ՖԻԶԻԿԱՅԻ ԻՆՍՏԻՏՈՒՏ

ԱՄԻՐԽԱՆՅԱՆ ՆԱՐԻՆԵ ՀՐԱՉԻԿԻ

ԼՈՒԾՈՒՅԹՆԵՐԻ ԱՑՐՄԱՄԲ ՍԻՆԹԵԶԻ ԿԻՆԵՏԻԿԱՅԻ ԵՎ ՄԵԽԱՆԻԶՄԻ ՀԵՏԱԶՈՏՈՒԹՅՈՒՆԸ ՄԵՏԱՂԻ ՆԻՏՐԱՏ - ՕՐԳԱՆԱԿԱՆ ՎԵՐԱԿԱՆԳՆԻՉ ՀԱՄԱԿԱՐԳԵՐՈՒՄ

Բ.00.04 - «Ֆիզիկական քիմիա» մասնագիտությամբ քիմիական գիտությունների թեկնածուի գիտական աստիճանի հայցման ատենախոսության

ՍԵՂՄԱԳԻՐ

ԵՐԵՎԱՆ 2025

A.B. NALBANDYAN INSTITUTE OF CHEMICAL PHYSICS NAS RA

AMIRKHANYAN NARINE

INVESTIGATION OF THE KINETICS AND MECHANISM OF SOLUTION COMBUSTION SYNTHESIS IN METAL NITRATE - ORGANIC REDUCTANT SYSTEMS

ABSTRACT

of Dissertation in 02.00.04 - "Physical chemistry" presented for the degree of candidate of chemical sciences

YEREVAN 2025

Ատենախոսության թեման հաստատվել է ՀՀ ԳԱԱ Ա.Բ. Նալբանդյանի անվան քիմիական ֆիզիկայի ինստիտուտում
Գիտական ղեկավար՝

քիմ . գիտ. թեկնածու Խաչատուր Վազգենի Մանուկյան

Պաշտոնական ընդդիմախոսներ՝

քիմ. գիտ. դոկտոր, պրոֆեսոր Ռոմիկ Սուրենի Հարությունյան
քիմ. գիտ. թեկնածու Անահիտ Ալեքսանի Սարգսյան

Առաջատար կազմակերպություն

ՀՀ ԳԱԱ Ֆիզիկական հետազոտությունների ինստիտուտ

Պաշտպանությունը կայանալու **է 2025 թ. Նոյեմբերի 7-ին, ժամը 14^{30}-ին** ՀՀ ԳԱԱ Ա.Բ. Նալբանդյանի անվան Քիմիական ֆիզիկայի ինստիտուտում գործող ՀՀ ԲԿԳԿ-ի 017 «Քիմիա» մասնագիտական խորհրդում (0014, Երևան, Պ Սևակի փ. 5/2):
Ատենախոսությանը կարելի է ծանոթանալ ՀՀ ԳԱԱ Ա.Բ. Նալբանդյանի անվան Քիմիական ֆիզիկայի ինստիտուտի գրադարանում:
Սեղմագիրն առաքված է 2025 թ. հոկտեմբերի 3-ին:

017 Մասնագիտական խորհրդի
գիտական քարտուղար, ք.գ.թ Մարիետա Կ. Զաքարյան

The subject of the dissertation is approved at A.B. Nalbandyan Institute of Chemical Physics, NAS RA
Scientific advisor:

Candidate of Chemical Sciences Khachatur V. Manukyan

Official opponents:

Doctor of Chemical Sciences, professor Romik S. Harutyunyan
Candidate of Chemical Sciences Anahit A. Sargsyan

Leading organization:

Institute of Physical Research of the NAS RA

Defense will takes place **on 7th of November 2025 at 14^{30}** on meeting of the special council of the HESC RA 017 "Chemistry", acting at A.B. Nalbandyan Institute of Chemical Physics NAS RA (0014, Yerevan, st. P. Sevak 5/2).
The PhD thesis is available at the library of A.B. Nalbandyan Institute of Chemical Physics NAS RA.
The abstract is sent out on October 3, 2025.
Scientific secretary of the 017 special council,
Candidate of Chemical Sciences Marieta K. Zakaryan

GENERAL DESCRIPTION OF THE WORK

Description of the work

Solution combustion synthesis (SCS) is a rapid, energy-efficient, and versatile route for producing nanostructured materials through the highly exothermic reaction of metal nitrates with organic fuels. This approach enables the preparation of oxides, metals, and, in some cases, nitrides, sulfides, and phosphides. SCS-derived materials find wide application in catalysis and in energy-storage and conversion technologies.

Despite these advantages, SCS faces key limitations: non-uniform product morphology, relatively low crystallinity, and difficulties in controlling product composition and potentially harmful gaseous products. These drawbacks stem primarily from the swift reaction rate and the limited understanding of the underlying kinetics and mechanisms. Consequently, elucidating the kinetics and mechanism of SCS is crucial for both fundamental science and industrial implementation. A deeper mechanistic understanding will enable optimization of synthesis conditions, prediction and control of the combustion behavior, and ultimately regulation of product quality.

Aim and problems of the work

This work aims to elucidate the mechanism and kinetics of SCS, explore their interrelationship, and determine how they govern the resulting products' microstructure, composition, and properties The study focuses on selected transition-metal systems chosen for their practical significance, including oxides (NiO, CoO, NiO–Fe_2O_3, NiO–CuO–Cu_2O), alloys (Ni_3Fe, NiCu), and a complex nitride (Ni_3CuN). Organic fuels, such as glycine ($C_2H_5NO_2$), citric acid ($C_6H_8O_7$), and hexamethylenetetramine ($C_6H_{12}N_4$), serve as reducers.

To accomplish these objectives, the following tasks are addressed:

- Investigate SCS reactions in the $Ni(NO_3)_2$–$C_2H_5NO_2$, $Ni(NO_3)_2$–$C_6H_8O_7$, $Ni(NO_3)_2$–$C_6H_{12}N_4$, $Co(NO_3)_2$–$C_6H_{12}N_4$, $Ni(NO_3)_2$–$Fe(NO_3)_3$–$C_6H_{12}N_4$, and $Ni(NO_3)_2$–$Cu(NO_3)_2$–$C_6H_{12}N_4$ systems.
- Examine how fuel type and ratio, oxidizer amount, reaction medium, pressure, and process mode affect the reaction mechanism and kinetic parameters during product formation.
- For relatively simple systems—$Ni(NO_3)_2$–$C_2H_5NO_2$, $Ni(NO_3)_2$–$C_6H_{12}N_4$, and $Co(NO_3)_2$–$C_6H_{12}N_4$—calculate adiabatic combustion temperatures and equilibrium product compositions as a function of the solution composition, and benchmark these results against experimental data.
- Develop and apply a method to evaluate the effective activation energy of SCS reactions. Assess how the heating rate of the initial solutions influences SCS kinetics and mechanisms, and analyze the composition of evolved gaseous products.
- Employ a suite of analytical techniques to correlate reaction mechanisms with the structural, compositional, and morphological characteristics of the solid products.

- Investigate low-temperature sintering of the nanopowder products and determine the physical and mechanical properties - including density, nanohardness, elastic modulus, and magnetic behavior - of selected compact samples.

Novelty of the work

- The chemical mechanism and kinetics of SCS processes, and the relationship between them, were comprehensively investigated in representative model systems enabling the controlled synthesis of oxides, metals, alloys, and complex compounds.
- Thermodynamic calculations established the equilibrium product compositions and the adiabatic combustion temperatures for the studied systems.
- Product formation follows a distinct sequence governed by the fuel-to-oxidizer ratio: fuel-lean solutions predominantly yield oxides; increasing the fuel content promotes the formation of metals or alloys; and high amounts of nitrogen-containing fuels favor the formation of complex nitrides. This trend is linked to the release of reducing gases (H_2, CH_4, N_2H_4) during excess-fuel decomposition.
- The interaction mechanisms in the $Ni(NO_3)_2$–$C_6H_{12}N_4$, $Co(NO_3)_2$–$C_6H_{12}N_4$, and $Ni(NO_3)_2$–$Cu(NO_3)_2$–$C_6H_{12}N_4$ systems were elucidated, revealing that the synthesis mechanism is controlled by the interaction of intermediate products formed during the decomposition of fuels and oxidizers.
- The Merzhanov–Khaikin method of kinetic analysis was applied to SCS reactions, demonstrating that the rate-limiting stage of combustion is the decomposition of nitrates.
- Combined thermal analysis and mass spectrometry provided detailed data on the mechanism and kinetics of the process for selected model systems.

Practical value of the work

- The studies enabled precise control over the synthesis process including - rate, reaction time, and conditions— enabled the production of homogeneous, fine-grained, and high-purity materials, including NiO, CoO, Ni, γ-Co, ε-Co, Ni_3Fe, and Ni_3CuN.
- High-density compact samples were obtained by sintering Ni and Co powders synthesized via SCS at relatively low temperatures (775 K and 1273 K). Notably, the formation and retention of the metastable γ-Co phase in the compact samples, typically prone to transformation into ε-Co, represent a significant achievement rarely attainable by conventional methods.
- Oxidation of metals and alloys during the post-combustion stage was successfully suppressed by maintaining an inert atmosphere: a pressure of 0.1–1.5 MPa in the self-propagating mode or a flow rate of 500 cm^3 min^{-1} in the volumetric combustion mode.
- Tailoring the initial composition, it was enables to synthesize a broad range of products: simple oxides (NiO, CoO), mixed oxides (NiO–Cu_2O, NiO–CuO, NiO–Fe_2O_3), pure metals (Ni, γ-Co), alloys (Ni_3Fe, CuNi, $Cu_{0.16}Ni_{0.86}$), and the complex nitride Ni_3CuN. Furthermore, in the $Co(NO_3)_2$–$C_6H_{12}N_4$ system, careful control of the cooling process enabled the formation of a metastable Co phase.

- In the $Ni(NO_3)_2$–$Cu(NO_3)_2$–$C_6H_{12}N_4$ system, employing a significant excess of fuel promoted the formation of the complex nitride Ni_3CuN during the cooling stage.

Content and structure of the work

The dissertation consists of an introduction, six chapters, conclusions, and a list of references. It is presented on one hundred and forty-three (143) pages, includes eight (8) tables, sixty-three (63) figures, and one hundred and fifty three (153) references.

Publications

The main part of the dissertation has been published in seven (7) articles in high-impact international peer-reviewed journals, one of which was published without co-authors, as well as in six (6) conference abstracts.

Chapter 1. Literature review

This chapter surveys the origins, scientific foundations, and practical applications of SCS. It provides a detailed analysis of the various SCS regimes, emphasizing both their distinguishing features and common principles. Particular attention is given to the precursors used in SCS, covering their selection criteria, reactivity, advantages, and classification into distinct groups. The review further examines available thermodynamic and kinetic data, analyzes the current understanding of SCS reaction mechanisms, and evaluates existing approaches to their description. It also identifies the classes of materials accessible through SCS and highlights how the synthesis regime and choice of precursors determine the microstructural characteristics of the final products. Finally, the chapter summarizes the advantages that make SCS a highly efficient and versatile method in modern materials science, while also addressing its key limitations and the need for continued research and methodological refinement.

Chapter 2. Experimental section

Model systems were selected that yield pure oxides and metals, alloys, and complex nitride-based phases. Experiments were performed under two combustion regimes: volume combustion and self-propagating combustion. In the volume combustion regime, reactions were carried out in borosilicate beakers under a continuous flow of inert gas (argon or nitrogen) to suppress unwanted oxidation and maintain stable combustion. In the self-propagating combustion regime, reactions were performed in paper boats placed inside a constant-pressure reactor. Thermocouples recorded combustion temperatures in both regimes, and in the self-propagating mode the propagation velocity of the combustion front was also measured.

To investigate the mechanism and kinetics of SCS processes, the model systems were subjected to thermal analysis using differential scanning calorimetry (DSC) and thermogravimetric analysis (TGA) under varying conditions. These techniques enabled identifying phase transitions, quantifying mass losses, and determining effective activation energies through established mathematical models.

The solid products were characterized by X-ray diffraction (XRD), with phase composition determined using international diffraction databases and refined through Rietveld analysis. Morphological features and microstructures were examined by high-resolution scanning electron microscopy (SEM), providing information on particle size, shape, and spatial distribution. Energy-dispersive X-ray spectroscopy (EDS) enabled local elemental analysis, while transmission electron microscopy (TEM) offered high-resolution imaging of nanocrystalline domains. The thermal stability of the combustion products and their structural changes (sintering) at elevated temperatures were evaluated using a High-Speed Temperature Scanner (HSTS). Additional characterization included specific surface area measurements (BET method), density determinations, nanoindentation for hardness and elastic modulus, and magnetic property measurements. This comprehensive suite of analyses allowed direct correlation between product properties, synthesis regimes, and the characteristics of the selected precursors.

Chapter 3. SCS process in $Ni(NO_3)_2$–fuel systems

In this chapter, SCS was studied in $Ni(NO_3)_2$ - organic fuel systems. In particular, the following reactions were considered in the nickel nitrate-glycine and nickel nitrate - HMTA (hexamethylenetetramine) systems:

$$Ni(NO_3)_2 + \frac{10}{9}\varphi\, C_2H_5NO_2 + \frac{5}{2}(\varphi - 1)\, O_2 = NiO + \frac{20}{9}\varphi\, CO_2 + \frac{25}{9}\varphi\, H_2O + \frac{5\varphi + 9}{9}\, N_2 \quad (1)$$

$$Ni(NO_3)_2 + \frac{5}{18}\varphi\, C_6H_{12}N_4 + \frac{5}{2}(\varphi - 1)\, O_2 = NiO + \frac{5}{3}\varphi\, CO_2 + \frac{5}{3}\varphi\, H_2O + \frac{5\varphi + 9}{9}\, N_2 \quad (2)$$

Thermodynamic calculations were carried out, in which the value of φ (fuel-to-oxidizer ratio) was varied within the range of 0.1 to 3, and the value of **n** within the range of 0 to 6 mol, taking into account the maximum amount of water in the nickel nitrate hydrate.

The calculations were performed at a pressure of 0.1 MPa, using two approaches - without oxygen and with oxygen participation. The results of the calculations with molecular oxygen participation for the nickel nitrate - glycine system are presented in Fig. 1. At low water contents, an increase in the value of φ leads to a rise in T_{ad}. The maximum value of T_{ad} is observed at φ = 3 and n = 0 (2480 K). The main gaseous products are CO_2 and N_2, whose equilibrium amounts increase in parallel with the growth of φ (for a given n value) and water vapor (not shown). Although CO_2 and N_2 are the predominant gaseous products, the formation of NO and CO is also observed in certain fuel-rich systems. In the gaseous products of fuel-rich systems, a small amount of H_2 is also detected (up to 0.19 mol). The amount of O_2 decreases with increasing φ, up to approximately φ ≈ 1. In fuel-rich systems (φ > 2) with low water content (n < 3), the amount of O_2 is slightly higher. The molecular oxygen present in the system mainly promotes the formation of NiO.

In the calculations without oxygen, the maximum T_{ad} (2000–2230 K) is recorded at φ ≈ 1 and n = 0. In all other cases, the temperature decreases with increasing values of the two variables.

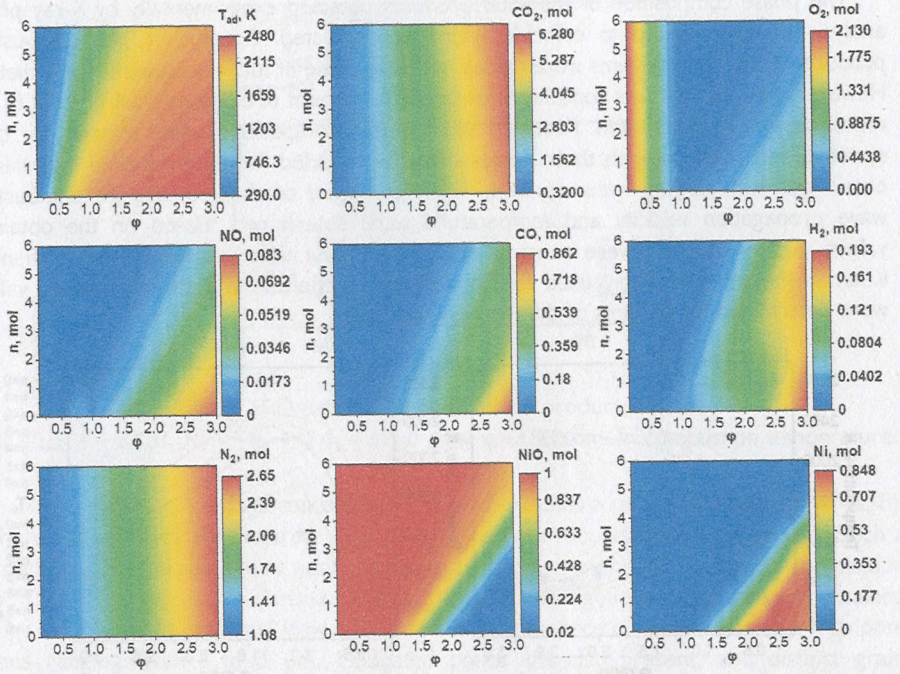

Fig. 1. Two-dimensional level plots for T_{ad} and equilibrium product for the $Ni(NO_3)_2 + \frac{10}{9}\varphi\, C_2H_5NO_2 + \frac{5}{2}(\varphi - 1)\, O_2 + n\, H_2O$ system depend on φ ratio and n (number of H_2O moles)

Similar calculations were also carried out for the nickel nitrate - urotropine system. For both systems, in order to compare the adiabatic combustion temperatures determined with and without oxygen participation to the maximum experimental combustion temperature, the results are presented in a single generalized graph (Fig. 2), as a function of the amount of water used in the system. The dashed curves correspond to the calculations with oxygen, while the solid curves correspond to the calculations without oxygen. The experimentally measured T_c values are close to the thermodynamically calculated T_{ad} values obtained without oxygen. Nevertheless, in the glycine system, the maximum experimental temperature is observed at φ = 1.25, while the maximum T_{ad} is calculated at φ = 1 (Fig. 2a).

As a result of vaporization, the gel retains 2 molecules of bound water. In this case, the difference between T_{ad} and T_c is about 500 K (Fig. 2a). For systems containing HMTA, the difference between T_c and T_{ad} is considerably larger (Fig. 2b). Taking into account that, the ignition temperature of HMTA - containing solutions is 470 ± 10 K, the gel formed after vaporization may contain 1–2 mol of bound water, and the corresponding difference between T_c and T_{ad} amounts to about 900 K over a relatively wide range of φ values.

The phase composition of the solid products obtained experimentally by X-ray phase analysis was also found to coincide with that calculated. Specifically, the combustion products of fuel-lean systems were oxides, whereas those of fuel-rich systems were metals. However, despite high fuel content, a considerable amount of oxide was still present in the nickel nitrate- HMTA system. Fuel-rich and fuel-lean compositions were selected for both systems, and solutions with these compositions were dried for different time intervals to obtain gels with varying water content. These gels were combusted, and the combustion wave propagation velocity and temperature were determined. Based on the obtained values, Arrhenius plots were constructed. For the first time, applying the Merzhanov–Khaitkin method commonly used for solid-phase reactions, the activation energy values were determined for systems of different compositions.

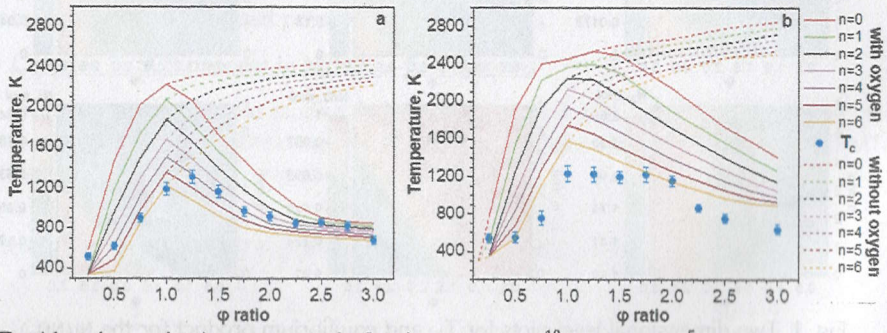

(T_c , blue data points) versus φ ratio for the $Ni(NO_3)_2 + \frac{10}{9}\varphi\ C_2H_5NO_2 + \frac{5}{2}(\varphi - 1)\ O_2 + n\ H_2O$ (a) and $Ni(NO_3)_2 + \frac{5}{18}\varphi\ C_6H_{12}N_4 + \frac{5}{2}(\varphi - 1)\ O_2 + n\ H_2O$ (b) systems. Plots also include calculated T_{ad} values (solid and dashed lines)

The high activation energy (E_a) values are characteristic of fuel-lean systems, where the final product is NiO. Although in the present work the E_a values were calculated considering thermal and mass transfer processes (macroscopic kinetics), it can be assumed that the activation energies may also be determined by certain rate-limiting stages affecting the combustion front velocity (V). The obtained values were compared with the decomposition activation energies of the starting materials (decomposition E_a of anhydrous nickel nitrate in air is 143–153 kJ·mol^{-1}; for glycine in nitrogen, 158 kJ·mol^{-1}; and for HMTA, 75 kJ·mol^{-1}). From these comparisons, it can be concluded that complex compounds are formed during the decomposition of the initial reagents, whose decomposition constitutes the rate-limiting step for these systems. Such a mechanism is referred to as the complexation–combustion mechanism. However, this hypothesis has not yet been experimentally confirmed and remains at the assumption stage.

In particular, in the nickel nitrate - HMTA system, X-ray phase analysis of the combustion products obtained from experiments carried out in a constant-pressure reactor under 3 MPa pressure has shown that in fuel-lean systems the combustion product is a metal oxide, while starting from φ = 1.5, pure metal is formed (Fig. 3).

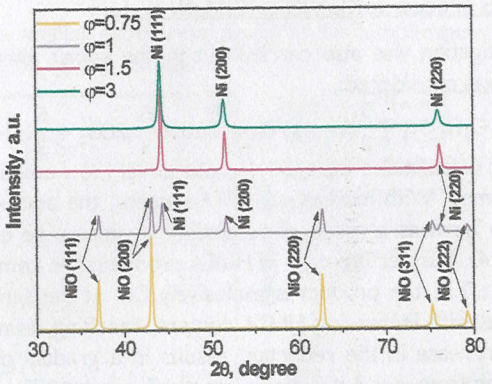

Fig. 3. XRD patterns of combustion products for the $Ni(NO_3)_2 + \frac{5}{18}\varphi\ C_6H_{12}N_4 + \frac{5}{2}(\varphi - 1)\ O_2 + n\ H_2O$ gelsFig. 2. Maximum combustion temperature

Nickel obtained from gel combustion at φ = 1.5 exhibits a porous structure (Fig. 4a, b), where the particles are sintered together and no grain boundaries are observed. Such a structure makes it possible to easily compact the product even at 773 K. After compaction at 773 K, a sample with a density of 90 ± 2% and a homogeneous structure was obtained (Fig. 4c). The cross-sectional view clearly shows the presence of certain porosity, with pore sizes ranging from 1 to 5 μm. Elongated pores are also present, and distinct grain boundaries between individual particles can be observed (Fig. 4d).

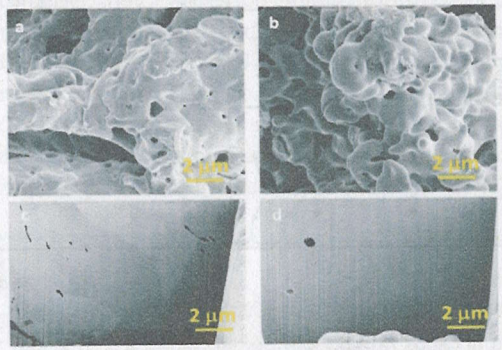

Fig. 4. SEM images of nanoscale Ni prepared by combustion of fuel - rich gels and sintered samples: Ni powder prepared at 0.3 (a) and 1.5 (b) MPa nitrogen pressures, sintered samples at 773 K (c) and 1275 K (d)

After compaction at 1275 K, denser samples with 95 ± 2% density were obtained, containing a limited number of pores (≈0.5 μm) (Fig. 4d). In the cross-sectional view, the grain boundaries are poorly expressed.

Chapter 4. SCS process in $Co(NO_3)_2$–$C_6H_{12}N_4$ system

A similar investigation was also carried out in the cobalt nitrate–HMTA system. The following reaction was considered:

$$Co(NO_3)_2 + \frac{5}{18}\varphi\, C_6H_{12}N_4 + \frac{5}{2}(\varphi - 1)\, O_2 = CoO + \frac{5}{3}\varphi\, CO_2 + \frac{5}{3}\varphi\, H_2O + \frac{5\varphi + 9}{9}\, N_2 \quad (3)$$

Thermodynamic calculations were carried out at very low amounts of HMTA (φ = 0.1–0.25), Co_3O_4 is formed. With increasing HMTA content, the amount of Co_3O_4 decreases, and CoO begins to form as a result of reduction. In the range φ = 0.5–1, the product consists solely of CoO. Further increase in HMTA promotes the complete reduction of CoO to the metal. At φ ≥ 1.5, the product is exclusively Co. At the same time, in the studied system T_{ad} increases with increasing HMTA content, reaching its maximum value (φ = 1, 2700 K). Further increase in the reductant results in a gradual decrease of T_{ad} (φ = 3, 1300 K), and starting from φ = 3 it remains practically unchanged.

The change in product composition as a function of fuel content was consistent with the experimentally obtained product composition. The combustion product of fuel-lean gels was CoO, whereas near φ = 1, the combustion product represented a mixture of γ-Co and CoO. In fuel-rich systems, CoO was reduced to metallic Co (Fig. 5a). It should be noted that, since the combustion temperature of fuel-rich gels (800–1600 K) is higher than the allotropic transformation temperature of cobalt, metastable γ-Co is formed. At the same time, the rapid cooling of the product prevents the γ→ε transformation.

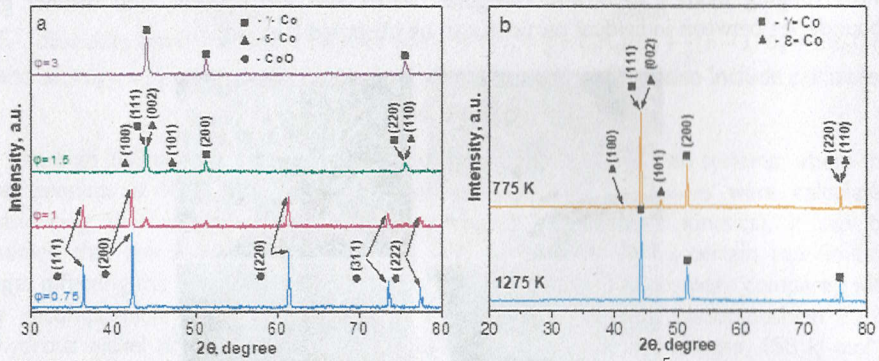

Fig.5. XRD patterns of combustion products of the $Co(NO_3)_2 + \frac{5}{18}\varphi\, C_6H_{12}N_4$ gels at different φ ratios (a) and samples sintered at 775 K and 1275 K (b)

SCS processes proceed quite rapidly; therefore, to correctly evaluate the mechanism, thermal treatment of gels with ratios of φ = 0.75 and φ = 1.5 was carried out under milder conditions than SCS. The gels were heated at 10–70 K·min^{-1}. The results of the study show that, for the two-component gels, the characteristic combustion reaction occurs at 450–550 K (Fig. 6). For the fuel-lean gel, the DSC curve obtained at a heating rate of 10 K·min^{-1}, in addition to the central characteristic intense exothermic peak (465

K), also includes two smaller exothermic peaks in the temperature ranges of 450–460 K and 480–500 K (Fig. 6a, green curve).

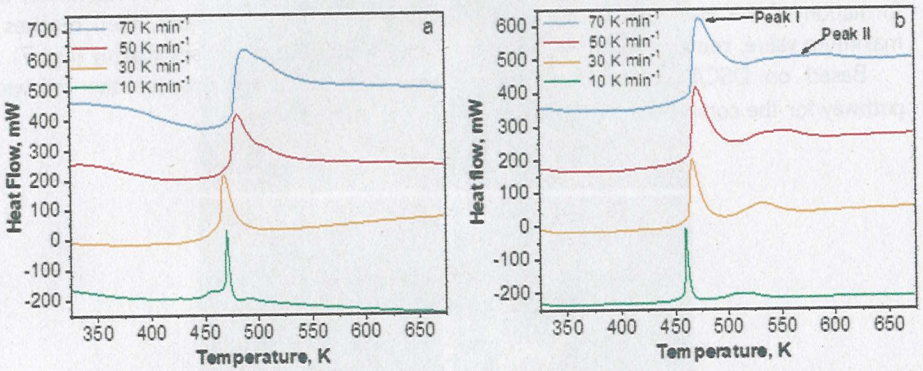

Fig. 6. DSC curves for $Co(NO_3)_2 + \frac{5}{18}\varphi\, C_6H_{12}N_4$ systems, when φ =0.75 (a) and φ =1.5 (b) at different heating rates

In the case of the fuel-rich gel, two characteristic exothermic peaks are observed: the most intense peak appears at 450 - 490 K (Peak I), while the second, less intense one, occurs at 490 - 575 K (Peak II). For both fuel-lean and fuel-rich gels, as the heating rate increases from 10 to 70 K·min^{-1}, the primary peak shifts to a higher temperature range, while the smaller peaks merge with the main one. By applying the Kissinger method to the prominent exothermic peaks, the E_a values for the transformation of the fuel-lean and fuel-rich gels were determined, yielding 96 ± 4 kJ·mol^{-1} and 205 ± 11 kJ·mol^{-1}, respectively.

When heating the gels at a rate of 30 K·min^{-1}, simultaneous mass-spectrometric analysis was also carried out (Fig. 7). According to the obtained results, the signals of CH_4^+(m/z = 16) and $N_2H_4^+$(m/z = 32) ions sharply increase, corresponding to the main exothermic stages of the DSC curves of both gels. However, in the case of the fuel-rich gel, the signals of these ions are comparatively more intense (Fig. 7b) than in the fuel-lean gel (Fig. 7a).

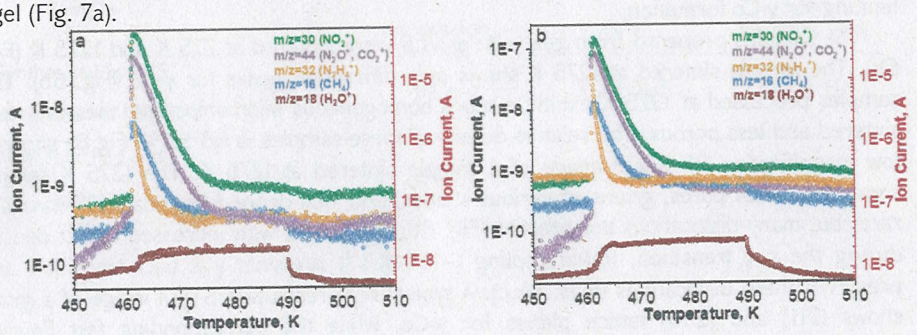

Fig. 7. Mass spectroscopy results for $Co(NO_3)_2 + \frac{5}{18}\varphi\, C_6H_{12}N_4$ systems, when φ =0.75 (a) and φ =1.5 (b) heated at 30 K min^{-1} rate

A sharp increase is also observed in the signals of NO_2^+(m/z = 30) and CO_2^+/N_2O^+(m/z = 44) ions, which are likewise associated with the primary exothermic process. However, their decrease occurs more slowly than the flow of CH_4^+ and $N_2H_4^+$ ions. Meanwhile, the formation of the H_2O^+(m/z = 18) ion begins later than the other ions, then reaches a maximum value, remains stable for a specific time, and finally decreases sharply (Fig. 7).

Based on DSC/MS measurements and literature data, we propose the following pathway for the combustion of $Co(NO_3)_2 + \frac{5}{18}\varphi\, C_6H_{12}N_4$solutions

$$Co(NO_3)_2 \rightarrow Co_3O_4 + NO_2 + O_2 \quad (4)$$

$$C_6H_{12}N_4 \rightarrow CH_4 + N_2H_4 + N_2 \quad (5)$$

$$CH_4 + O_2(NO_2) \rightarrow CO_2 + H_2O\ (+N_2) \quad (6)$$

$$N_2H_4 + O_2(NO_2) \rightarrow N_2 + H_2O \quad (7)$$

$$2Co_3O_4 + N_2H_4 = 6CoO + N_2 + 2H_2O \quad (8)$$

$$4Co_3O_4 + CH_4 = 12CoO + CO_2 + 2H_2O \quad (9)$$

$$2CoO + N_2H_4 = 2Co + N_2 + 2H_2O \quad (10)$$

$$4CoO + CH_4 = 4Co + CO_2 + 2H_2O \quad (11)$$

Dehydration of cobalt nitrate hexahydrate occurs at 300–450 K, followed by decomposition of the anhydrous salt at ~450 K, producing Co_3O_4 (4). Thermodynamic calculations predict Co_3O_4 formation at $\varphi < 0.5$. Meanwhile, fuel sublimation/decomposition releases CH_4, N_2H_4, and N_2 (5). The exothermic peak at 450–460 K in fuel-lean gels (Fig. 6a, 7a) corresponds to Co_3O_4 reduction to CoO via reactions (8) and (9), confirmed by XRD (Fig. 5). Increasing the heating rate merges this step with the primary exothermic stage. CH_4 and N_2H_4 further react with NO_2 and O_2, forming hypergolic mixtures that provide the main combustion heat ((6), (7)). The apparent activation energy of this stage is 96 ± 4 kJ·mol^{-1}, higher than that of cobalt nitrate decomposition (59 ± 5 kJ·mol^{-1}) and close to the sublimation heat of $C_6H_{12}N_4$ (75 ± 3 kJ·mol^{-1}), suggesting fuel sublimation/gas-phase decomposition is rate-limiting.

For fuel-rich gels ($\varphi \geq 1.5$), thermodynamics and XRD confirm γ-Co formation (Fig. 5). CoO reduction by CH_4 and N_2H_4 proceeds via reactions (10) and (11). Reaction (11) activation energy (155 ± 20 kJ·mol^{-1}) is close to the apparent value for the primary exothermic stage (205 ± 11 kJ·mol^{-1}), indicating that CoO reduction ((10), (11)) is rate-limiting for γ-Co formation.

The samples prepared from gels with φ =1.5 were sintered at 775 K and 1275 K (Fig. 6b). The sample sintered at 1275 K shows only diffraction peaks for γ-Co (Fig. 6b). The samples processed at 1275 K exhibit a more homogeneous microstructure: they are well-sintered and less porous. The relative density of these samples is 88 ±3 %. Fig.8a shows a low magnification BF STEM image of a sample sintered at 1275 K. The 1275 K sample shows few small pores, grains of various shapes, and well-defined boundaries. Twins are rare, but many dislocations are present (Fig. 8b), consistent with increased defect density during the ε→γ transition. Rapid cooling (~150 K·s^{-1}) prevents γ→ε back-transition and preserves these dislocations (Figs. 8b,c). A typical high-resolution STEM image of a grain shows (211) and (200) lattice planes for γ-Co, while the corresponding fast Fourier transform (FFT) of the image exhibits (111), (002), and (220) planes (Figs. 8d).

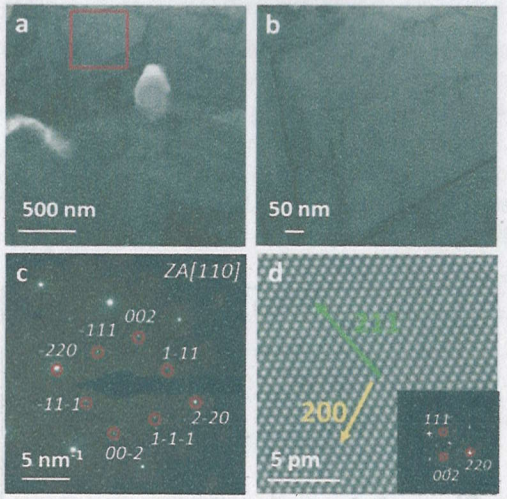

Fig. 8. TEM analysis of a sample sintered at 1275 K: Low (a) and high magnification (b) BF STEM image of a grain, SAED pattern for the same grain (c), and high-resolution HAADF STEM image (d) of the γ-Co grain with FFT pattern (inset)

Nanoindentation tests were conducted to determine the elastic modulus and nanohardness of the sintered samples. We also conducted nanoindentation measurements for a pure ε-Co sample. The resaults shown in Table 1. These results indicate that sintered samples containing γ-Co exhibit relatively higher Young's moduli than ε-Co samples at similar grain sizes. We can expect that mechanical properties of γ-Co could be improved with more dense samples due to more complete particle bonding.

Table 1 Nanohardness and Young's modulus of samples.

Sample	Relative density, %	Phase composition	Nanohardnes, GPa	Young's modulus, GPa
Synthesized by SCS and sintered at 1275 K	88	γ-Co	3.2 ±0.15	129.0 ±9
Melt solidified and rolled	100	ε-Co	3.9 ±0.3	93.8 ±3

Chapter 5. SCS process in $Ni(NO_3)_2$–$Fe(NO_3)_3$–$C_6H_{12}N_4$ system

To study the regularities of SCS in a multicomponent system and simultaneously obtain pure Ni_3Fe intermetallic compound in a single step, the $3Ni(NO_3)_2{\cdot}6H_2O$–$Fe(NO_3)_3{\cdot}9H_2O$–$\varphi C_6H_{12}N_4$ system was investigated, keeping the nitrate content constant and varying the amount of fuel (φ). The value of φ was changed within the range of 1 to 12. At $n \leq 1$ and $n \geq 12$ values, combustion limits were observed. XRD analysis of the products obtained at different fuel contents showed that pure Ni_3Fe phase is formed at $\varphi = 6$ (Fig. 9). At $\varphi = 4$, in addition to the Ni_3Fe alloy, traces of the Ni_3FeN complex nitride were also detected in the product.

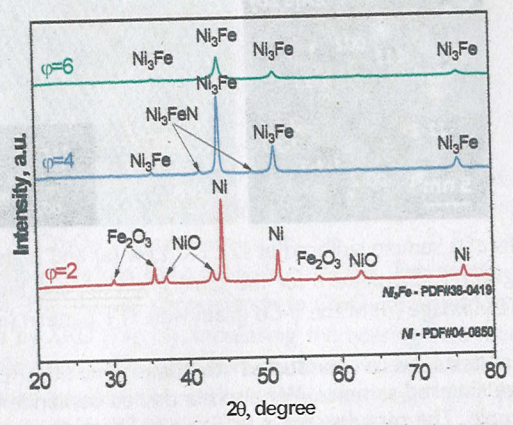

Fig. 9. X-ray diffraction patterns of the combustion products of the $3Ni(NO_3)_2{\cdot}6H_2O$-$Fe(NO_3)_3{\cdot}9H_2O$-$\varphi C_6H_{12}N_4$ system for different values of φ

To understand the possible transformations in the reaction gel and the mechanism of SCS, TG analysis was carried out by heating the materials under milder and controlled conditions. According to the obtained results (Fig. 10), in a nitrogen atmosphere, hexamethylenetetramine decomposes in the temperature range of 413–513 K, completely converting into gases. Under the same conditions, the decomposition of $Fe(NO_3)_3{\cdot}9H_2O$ starts at 323 K. Two characteristic stages are observed, forming Fe_2O_3 at 473 K. The decomposition of $Ni(NO_3)_2{\cdot}6H_2O$ starts at 403 K and, according to literature data, is accompanied by dehydration, leading to $Ni(NO_3)_2{\cdot}2H_2O$. The latter decomposes in the range of 583–653 K to form NiO.The TG curve of the mixture with optimal composition shows that intensive interaction occurs at 483–493 K. In this range, as mentioned, Fe_2O_3, $Ni(NO_3)_2{\cdot}2H_2O$, and a mixture of gases are present in the system. Therefore, it can be assumed that Ni_3Fe is formed due to the interaction of these substances. Alternatively, a complex intermediate compound may first form from the interaction of the starting components, and its decomposition followed by the direct interaction of the released metals leads to the formation of the target Ni_3Fe alloy.

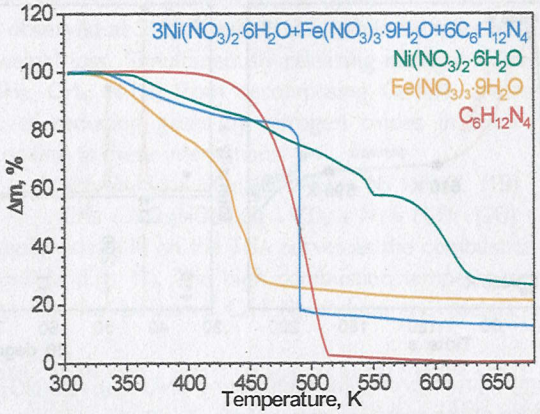

Fig. 10. TG curves of the reaction mixture and starting materials with the composition $3Ni(NO_3)_2{\cdot}6H_2O + Fe(NO_3)_3{\cdot}9H_2O + 6C_6H_{12}N_4$

When $\varphi = 6$, the Ni: Fe ratio is 2.7:1. According to the results of local X-ray spectral analysis of Ni_3Fe, it lies within the single-phase region of the Fe–Ni phase diagram corresponding to the Ni_3Fe intermetallic compound. On the other hand, microstructural investigations showed that the product is an agglomerate with a porous structure. The magnetization of the obtained Ni_3Fe intermetallic compound is 50 ± 0.5 $A{\cdot}m^2{\cdot}kg^{-1}$, which allows it to be classified among superparamagnetic compounds.

Chapter 6. SCS process in $Ni(NO_3)_2$–$Cu(NO_3)_2$–$C_6H_{12}N_4$ system

In this chapter, the combustion process was studied in t he $3Ni(NO_3)_2$–$Cu(NO_3)_2$–$5C_6H_{12}N_4$ system with the aim of preparing Ni_3CuN complex nitride with an antiperovskite cubic structure. A representative time-temperature profile for the combustion process of the $3Ni(NO_3)_2 + Cu(NO_3)_2 + 5C_6H_{12}N_4$ solution exhibits five distinct stages: preheating, rapid self-heating (combustion), the first cooling, a constant temperature plateau, and the second cooling (Fig. 11a). The inflection point between the heating and combustion stages marks the ignition temperature (T_{ig}), which is 400 K. During the combustion stage, the temperature increases at approximately 50 K/s rate, reaching a T_{max} of 845 K. In the first cooling stage, the product cools at ~4.5 K/s until the temperature stabilizes at around 600 K for about one minute. After this plateau, the material undergoes a second cooling stage at a rate of approximately 1.5 K/s. The XRD pattern for the SCS product closely matches the calculated diffraction pattern (ICDD PDF-2 #01–084–8255) for cubic ($Pm\bar{3}m$) Ni_3CuN (Fig. 11b). The product features uniform near-spherical agglomerates with an average size of approximately 360 ± 140 nm.

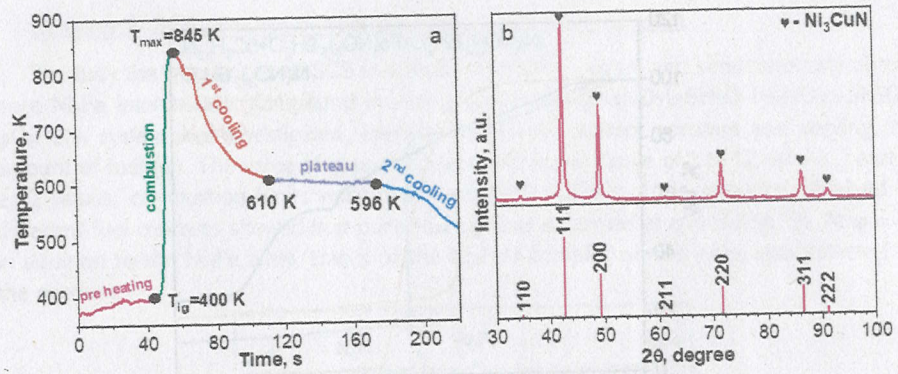

Fig. 11. A time-temperature profile for combusting $3Ni(NO_3)_2$+$Cu(NO_3)_2$+$5C_6H_{12}N_4$ solution (a) and XRD pattern of the resulting material along with the calculated diffraction pattern (ICDD PDF 2 #01-084-8255) for Ni_3CuN (b)

To further investigate the SCS reaction dynamics, TGA analysis of the $3Ni(NO_3)_2$ + $Cu(NO_3)_2$ + $5C_6H_{12}N_4$ gel was conducted up to 850 K with heating rates ranging from 5 to 30 K min^{-1} (Fig. 12). The TGA curves revealed five distinct stages, each reflecting specific thermal events and chemical transformations.

Stage I, occurring between 300 and 470 K, corresponds to the dehydration of crystal hydrates in copper nitrate and nickel nitrate. For copper nitrate, dehydration produces $Cu(NO_3)_2{\cdot}3Cu(OH)_2$ along with the release of NO_2 and water vapor:

$$Cu(NO_3)_2{\cdot}3H_2O \rightarrow Cu(NO_3)_2{\cdot}3Cu(OH)_2 + NO_2 + H_2O \quad (13)$$

Nickel nitrate hexahydrate undergoes a similar dehydration process, forming $Ni(NO_3)_2{\cdot}2H_2O$, NO_2 and water vapor:

$$Ni(NO_3)_2{\cdot}6H_2O \rightarrow Ni(NO_3)_2{\cdot}2H_2O + NO_2 + H_2O \quad (14)$$

Around 470 K, stage II begins with the decomposition of $Cu(NO_3)_2{\cdot}3Cu(OH)_2$ to form CuO, NO_2, and water vapor. This decomposition is also a ccompanied by the catalytic conversion of NO_2 on the surface of CuO, generating NO and O_2:

$$Cu(NO_3)_2{\cdot}3Cu(OH)_2 \rightarrow CuO + NO_2\ (NO + O_2) + H_2O \quad (15)$$

$$NO_2 \xrightarrow{Cu} NO{+}O_2 \quad (16)$$

Notably, stages II and III in the TGA curves align with the reported decomposition temperature range of $C_6H_{12}N_4$. Depending on the atmosphere, $C_6H_{12}N_4$ undergoes either endothermic sublimation and gas-phase decomposition between 460 and 600 K or exothermic decomposition, yielding solid or oily organic matter ($C_xN_yH_z$) along with gaseous products such as NH_3, CH_4, N_2H_4, and N_2:

$$C_6H_{12}N_4 \rightarrow N_2H_4 + CH_4 + N_2 + C_xN_yH_z \quad (17)$$

The onset of stage III, occurring around 530 K, corresponds to the thermal decomposition of $Ni(NO_3)_2{\cdot}2H_2O$, which produces NiO, NO_2, and water vapor:

$$Ni(NO_3)_2{\cdot}2H_2O \rightarrow NiO + NO_2 + H_2O \quad (18)$$

The heating rate significantly influences the dynamics of stage III. A more gradual weight decrease is observed at 5–15 K min_{-1} rates, while samples heated at 20–30 K min exhibit an abrupt weight loss. Simultaneously releasing nitrogen oxides from nitrates and reducing gases (NH_3, CH_4, N_2H_4) from decomposing $C_6H_{12}N_4$ creates a hypergolic gas mixture. Oxidation of reducing gases by nitrogen oxides in such mixtures generates significant heat according to these interactions:

$$NH_3\ (N_2H_4) + NO_2(NO, N_2O) \rightarrow N_2 + H_2O \quad (19)$$

$$CH_4 + NO_2(NO,N_2O) \rightarrow CO_2 + N_2 + H_2O \quad (20)$$

Therefore, we assign stage III on the TGA curves as the combustion stage observed on time-temperature profile (Fig. 11). The high combustion temperatures and availability of reducing gases due to the excessive $C_6H_{12}N_4$ reduce the metals according to these reactions:

$$CuO + CH_4\ (NH_3, N_2H_4) \rightarrow Cu_2O + CO_2(g)\ (N_2(g)) + H_2O \quad (21)$$

$$Cu_2O + CH_4\ (NH_3, N_2H_4) \rightarrow Cu + CO_2\ (N_2) + H_2O \quad (22)$$

$$NiO + CH_4\ (NH_3, N_2H_4) \rightarrow Ni + CO_2\ (N_2) + H_2O \quad (23)$$

Next, the interaction of metals forms $Cu_{0.14}Ni_{0.86}$, which eventually converts into a relatively copper-rich Ni-Cu alloy:

$$Cu + Ni \rightarrow Cu_{0.14}Ni_{0.86} + Cu \rightarrow Ni\text{-}Cu \quad (24)$$

We postulate that Ni_3CuN formation occurs in stage IV, corresponding to a plateau in the time-temperature profiles (Fig. 11a). The Ni-Cu alloy converts into Ni_3CuN due to the supply of nitrogen-containing species of decomposing $C_xN_yH_z$:

$$Ni\text{-}Cu \xrightarrow{N\ (CxNyHz)} Ni_3CuN \quad (25)$$

Stage V in the TGA curves can be attributed to several processes: oxidation of carbonaceous residues and the thermal decomposition of the formed Ni_3CuN. The thermal analysis of SCS-derived Ni_3CuN supports this assignment, showing decomposition and nitrogen removal.

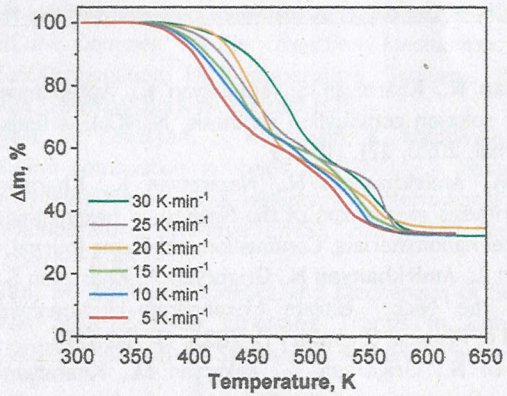

Fig.12. TGA analysis results of $3Ni(NO_3)_2$ +$Cu(NO_3)_2$ +$5C_6H_{12}N_4$ gel at 5, 10, 15, 20, 25, 30 K/s heating rates

The formation of Ni_3CuN through this SCS mechanism involves a sequential process: oxide formation, reduction to metals, alloying, and nitridation.

Conclusion

1. The key controlling parameters of the SCS process are the fuel type and fuel–oxidizer ratio, which directly influence the combustion temperature, chemical composition, and microstructure of the synthesized materials.
2. For the investigated SCS systems, the effective activation energies were determined characterizing the decomposition of the precursors or intermediate complex compounds.
3. The maximum temperature attained during SCS is governed by the heat released from the interaction of nitrogen oxides (N_2O, NO, NO_2), formed via nitrate decomposition, with the reducing gases (N_2H_4, CH_4) generated by fuel decomposition.
4. By varying the amount of fuel - and consequently the concentration of reducing gases such as CH_4 and N_2H_4 - it is possible to control the final product composition, enabling the selective synthesis of metal oxides, free metals, and/or alloys.
5. Nickel and cobalt nanopowders prepared by SCS demonstrate high sinterability at low temperatures (≤1273 K). Short-term thermal treatment of these powders produced compact samples with relative densities exceeding 90%.
6. Rapid cooling successfully preserved the high-temperature metastable γ-Co phase, which exhibits superior magnetic and mechanical properties, preventing its transformation into the thermodynamically stable ε-Co phase at lower temperatures.
7. In the nickel–copper nitrates/hexamethylenetetramine system, nitrogen-containing intermediate products generated during fuel decomposition reacted with the NiCu alloy formed in the combustion wave, resulting in the synthesis of the complex nitride Ni_3CuN—an antiperovskite material with promising catalytic and magnetic applications.

The main results of the dissertation were published in the following works

Articles:

1. **Amirkhanyan N.,** Kharatyan S., Manukyan K., Aprahamian A, Thermodynamics and kinetics of solution combustion synthesis: $Ni(NO_3)_2$ + fuels systems, Combustion and Flame Journal, 2020, 221, 110-119
2. Zakaryan M., **Amirkhanyan N.**, Nazaretyan K., Kharatyan S., Manukyan K., Combustion synthesis mechanism of the $Ni(NO_3)_2$ + hexamethylenetetramine solutions to prepare nickel nanomaterials, Combustion and Flame Journal, 2023, 257, 113049
3. Arzumanyan A., **Amirkhanyan N.**, Grigoryan Y., Kharatyan S., DTA/TG Study of the Interaction in the Nickel Nitrate Hexahydrate–Hexamethylenetetramine System, Russian Journal of Physical Chemistry B, 2023, 17, 122-127
4. **Amirkhanyan N.**, Grigoryan Y., Zakaryan M., Kharatyan A., Gyulasaryan H., Harutyunyan A., Preparation of the Ferromagnetic Intermetallic Compound Ni_3Fe by Solution Combustion Synthesis, Journal of Contemporary Physics (Armenian Academy of Sciences), 2023, 58, 299-304

5. **Amirkhanyan N.**, Zakaryan M., Kharatyan S., Yeghishyan A., Zhukovskyic M., Aprahamian A., Manukyan K., Stabilization of Metastable γ-Co: Combustion Synthesis and Rapid Processing, Materials Chemistry and Physics, 2024, 319, 129368
6. **Amirkhanyan N.**, Solution Combustion Synthesis and Kinetic Measurements in $Ni(NO_3)_2$–$C_6H_8O_7$ System. Preparation of Nickel Powder, International Journal of Self-Propagating High-Temperature Synthesis, 2024, 33, 100-108
7. Zakaryan M., **Amirkhanyan N.**, Kharatyan S., Aprahamian A., Manukyan K., Formation mechanism and kinetics of Ni_3CuN complex nitride in solution combustion synthesis, Combustion and Flame, 2025, 277, 114195

Theses:

1. **N. Amirkhanyan**, S. Kharatyan, K. Manukyan, Kinetic Measurements for solution combustion synthesis, XV International Symposium on Self-Propagation High-temperature Synthesis, 2019, 16-20 September, Russia, Moscow, Book of abstract p.15-16
2. **N. Amirkhanyan**, M. Zakaryan, A. Harutyunyan, Synthesis of Nanoscale Antiperovskite Complex Nitrides for Catalytic and Magnetic Applications, 15th International Ceramics Congress, 2022, 20-24 June, Italy, Perugia, Book of abstract C:P16
3. **N. Amirkhanyan**, M. Zakaryan, Synthesis of Intermetallic Ni3Fe compound for Magnetic Applications by Solution Combustion Synthesis Method, New Emerging Trends in Chemistry Conference (NewTrendsChem-2023), 2023, 24-28 September, Armenia, Yerevan, Book of abstract p.107
4. M. Zakaryan, **N. Amirkhanyan**, Solution Combustion Synthesis of the Ni3CuN Antiperovskite Battery Material, New Emerging Trends in Chemistry Conference (NewTrendsChem-2023), 2023, 24-28 September, Armenia, Yerevan, Book of abstract p.70
5. M. Zakaryan, **N. Amirkhanyan**, K. Manukyan, S. Kharatyan, Solution Combustion Synthesis of Ni3CuN Complex Nitride: Reaction Mechanism, XVI International Symposium of Self-Propagation High-temperature Synthesis (SHS), 2024, 9-13 September, Armenia, Yerevan, Book of abstract p.16
6. **N. Amirkhanyan**, M. Zakaryan, S. Kharatyan, K. Manukyan, The kinetics and mechanism of solution combustion synthesis in $Ni(NO_3)_2$ + hexamethylenetetramine and $Co(NO_3)_2$ + hexamethylenetetramine systems, XVI International Symposium of Self-Propagation High-temperature Synthesis (SHS), 2024, 9-13 September, Armenia, Yerevan, Book of abstract p.86,
7. **N. Amirkhanyan**, M. Zakaryan, Kinetics and Mechanism of Solution Combustion Synthesis in Model Systems, New Emerging Trends in Chemistry Conference (NewTrendsChem-2025), 2025, 21-25 September, Armenia, Yerevan, Book of abstract p.117

ԱՄԻՐԽԱՆՅԱՆ ՆԱՐԻՆԵ ՀՐԱՉԻԿԻ

ԼՈՒԾՈՒՅԹՆԵՐԻ ԱՅՐՄԱՄԲ ՍԻՆԹԵԶԻ ԿԻՆԵՏԻԿԱՅԻ ԵՎ ՄԵԽԱՆԻԶՄԻ ՀԵՏԱԶՈՏՈՒԹՅՈՒՆԸ ՄԵՏԱՂԻ ՆԻՏՐԱՏ - ՕՐԳԱՆԱԿԱՆ ՎԵՐԱԿԱՆԳՆԻՉ ՀԱՄԱԿԱՐԳԵՐՈՒՄ

ԱՄՓՈՓԱԳԻՐ

Լուծույթների այրմամբ սինթեզը (ԼԱՍ) հանդիսանում է արագ, արդյունավետ, էներգիախնայող, նորարարական մեթոդ նանոկառուցվածքային նյութերի ստացման համար: ԼԱՍ պրեցեսի հիմքում ընկած է մետաղների լուծելի աղերի՝ մասնավորապես նիտրատների (օքսիդիչ) և օրգանական վերականգնիչների (վառելիք) միջև ընթացող էկզոթերմ փոխազդեցությունը: ԼԱՍ պրոցեսը հնարավորություն է տալիս ստանալ հիմնականում օքսիդներ, մետաղներ, երբեմն նյութերի այլ դասեր՝ նիտրիդներ, սուլֆիդներ, ֆոսֆիդներ՝ բազմազան կիրառությունների համար: Մասնավորապես, ԼԱՍ-ով ստացված բազմաթիվ պարզ և բարդ օքսիդներ կիրառվում են որպես կատալիզատորներ գազերի օքսիդացման, ջրի և օրգանական նյութերի քայքայման ռեակցիաներում: ԼԱՍ պրոցեսով ստացված նյութերը լայն կիրառություն ունեն էներգիայի պահպանման և փոխակերպման ոլորտներում որպես մարտկոցների, սենսորների, գերհաղորդիչների բաղադրիչներ և այլն:

Գնալով աճում է հետաքրքրությունն այս եղանակով նյութերի ստացման նկատմամբ, սակայն ԼԱՍ պրոցեսն ունի որոշակի սահմանափակումներ՝ կապված արգասիքի կառուցվածքային համասեռության, երբեմն անբավարար բյուրեղական կառուցվածքի, դժվար կառավարելի բաղադրության, անջատվող գազերի կազմի և այլնի հետ: Այդ սահմանափակումները պայմանավորված են ԼԱՍ պրոցեսների կինետիկայի և մեխանիզմի, դրանց միջև կապի ոչ բավարար իմացությամբ: Մեխանիզմի և կինետիկայի վերաբերյալ մեծաթիվ տվյալների առկայությունը հնարավորություն կտա օպտիմալացնել սինթեզի պայմանները, կանխատեսել այրման ընթացքը և արագությունը՝ բերելով պրոցեսի կառավարմանը, ինչպես նաև հնարավոր կլինի կառավարել ստացվող նյութերի կառուցվածքը, որակը, անջատվող գազերի կազմը և քանակը:

Աշխատանքի նպատակն է. ուսումնասիրել ընտրված համակարգերում ԼԱՍ պրոցեսների մեխանիզմն ու կինետիկան, բացահայտել մեխանիզմի և կինետիկայի միջև կապը, դրանց ազդեցությունը արգասիքի միկրոկառուցվածքի, բաղադրության, հատկությունների վրա այնպիսի համակարգերում, որոնք բերում են օքսիդների, համաձուլվածքների և բարդ նիտրիդային միացության առաջացման:

Իրականացված հետազոտություններից ստացվել են հետևյալ հիմնական արդյունքները՝

- ԼԱՍ-պրոցեսի հիմնական կառավարող պարամետրերն են վառելիքի տեսակը և վառելիք - օքսիդիչ հարաբերակցությունը, որոնք ուղղակիորեն ազդում են այրման ջերմաստիճանի, ստացվող նյութերի քիմիական բաղադրության և միկրոկառուցվածքի վրա:

- Հետազոտված ԼԱՍ համակարգերում որոշվել են պրոցեսի ակտիվացման էներգիայի էֆեկտիվ արժեքները, որոնք բնութագրում են ելանյութերի (կամ միջանկյալ կոմպլեքս միացությունների) քայքայումը:
- ԼԱՍ-պրոցեսի առավելագույն ջերմաստիճանը պայմանավորված է ելային նիտրատների քայքայումից առաջացած ազոտի օքսիդների (N_2O, NO, NO_2) և վառելիքի քայքայման արդյունքում առաջացած վերականգնիչ գազերի (N_2H_4 և CH_4) փոխազդեցության ջերմէֆեկտով:
- Ցույց է տրվել, որ ԼԱՍ համակարգերում վառելիքի (վերականգնող գազերի՝ CH_4, N_2H_4) քանակի փոփոխությամբ կարելի է կարգավորել նպատակային արգասիքների բաղադրությունը՝ ստանալով ինչպես մետաղների օքսիդներ, այնպես էլ մետաղներ և/կամ համաձուլվածքներ:
- ԼԱՍ եղանակով ստացված նիկելի և կոբալտի նանոփոշիները ցուցաբերում են բարձր եռակալման ունակություն ցածր ջերմաստիճաններում (≤1273 Կ): Դրանց կարճատև ջերմային մշակմամբ ստացվել են 90%-ից բարձր հարաբերական խտությամբ կոմպակտ նմուշներ:
- Այրման արգասիքների արագ սառեցումը հնարավորություն է տվել պահպանել բարձրջերմաստիճանային, մետակայուն γ-Co ֆազը՝ շրջանցելով դրա փոխարկումը ցածր ջերմաստիճանում թերմոդինամիկորեն կայուն ε-Co-ի:
- Նիկելի և պղնձի նիտրատներ - ուրոտրոպին համակարգում վերջինիս քայքայման արդյունքում առաջացած ազոտ պարունակող միջանկյալ արգասիքների և այրման ալիքում առաջացած NiCu համաձուլվածքի փոխազդեցության արդյունքում սինթեզվել է Ni_3CuN բարդ նիտրիդային ֆազը:

АМИРХАНЯН НАРИНЕ ГРАЧИКОВНА

ИССЛЕДОВАНИЕ КИНЕТИКИ И МЕХАНИЗМА ПРОЦЕССОВ СИНТЕЗА ГОРЕНИЕМ РАСТВОРОВ В СИСТЕМАХ НИТРАТ МЕТАЛЛА – ОРГАНИЧЕСКИЙ ВОССТАНОВИТЕЛЬ

РЕЗЮМЕ

Синтез горением растворов (СГР) представляет собой быстрый, энергоэффективный и инновационный метод получения наноструктурированных материалов на основе экзотермического взаимодействия солей металлов — главным образом нитратов - с органическими восстановителями (топливами). Этот подход позволяет получать оксиды, металлы, а в ряде случаев также нитриды, сульфиды и фосфиды. Материалы, синтезированные методом СГР, широко применяются в катализе (окисление газов, разложение воды, деградация органических соединений), а также в области накопления и преобразования энергии - в батареях, сенсорах, сверхпроводниках и др.

Несмотря на очевидные преимущества, метод СГР имеет ряд ограничений, таких как неоднородность структуры, недостаточная кристалличность и трудности

управления составом продуктов и природой выделяющихся газов. Эти недостатки в основном связаны с чрезвычайно высокой скоростью протекания реакций и ограниченным пониманием их кинетики и механизмов.

Поэтому исследование кинетики и механизма процессов СГР имеет важное научное и практическое значение. Более глубокие знания позволят оптимизировать условия синтеза, прогнозировать и контролировать течение горения, а также регулировать структуру и качество получаемых материалов. Это создаст основу для преодоления существующих ограничений и расширит возможности применения метода СГР в различных технологических областях.

Цель работы — исследовать механизм процессов СГР в выбранных системах, их кинетику, взаимосвязь механизма и кинетики, а также их влияние на микроструктуру, состав и свойства продукта в таких системах, которые приводят к образованию оксидов, сплавов и сложных нитридных соединений.

Основные результаты проведённых исследований:

- Установлено, что основными управляющими параметрами процесса СГР являются тип топлива и соотношение топливо–окислитель, которые напрямую влияют на температуру горения, химический состав и микроструктуру получаемых материалов.
- В исследованных системах СГР определены эффективные значения энергии активации процесса, характеризующие разложение исходных веществ (или промежуточных комплексных соединений).
- Максимальная температура СГР-процесса обусловлена тепловым эффектом взаимодействия оксидов азота (N_2O, NO, NO_2), образующихся при разложении исходных нитратов, с восстановительными газами (N_2H_4 и CH_4), возникающими в результате разложения топлива.
- Установлено, что изменением количества топлива (восстановительных газов CH_4, N_2H_4) в системах СГР можно регулировать состав целевых продуктов, получая как оксиды металлов, так и металлы и/или сплавы.
- Нанопорошки никеля и кобальта, полученные методом СГР, проявляют высокую способность к спеканию при низких температурах (≤1273 К). Кратковременной термообработкой из них были получены компактные образцы с относительной плотностью выше 90%.
- Быстрое охлаждениепродуктов сгорания позволило сохранить высокотемпературную метастабильную γ-Co фазу, обладающую более высокими магнитными и механическими свойствами, минуя её превращение в термодинамически устойчивую ε-Co фазу при низких температурах.
- В системе нитратов никеля и меди - уротропина в результате взаимодействия азотсодержащих промежуточных продуктов разложения последнего с образовавшимся в пламени сплавом NiCu синтезирована сложная нитридная фаза Ni_3CuN, представляющая собой перспективный антиперокситный материал для каталитических и магнитных применений.